Computers and Structures 90–91 (2012) 145–152

Contents lists available at SciVerse ScienceDirect

Computers and Structures

journal homepage: www.elsevier.com/locate/compstruc

A numerical and experimental study of bearing stiffness of drilled shafts socketed in heterogeneous rock

Jae H. Chung [a,*], Jeongsoo Ko [b], Harald Klammler [c], Michael C. McVay [b], Peter Lai [d]

[a] University of Florida, Bridge Software Institute, Department of Civil and Coastal Engineering, P.O. Box 116580, Gainesville, FL 32611, USA
[b] University of Florida, Department of Civil and Coastal Engineering, USA
[c] Federal University of Bahia, Department of Environmental Science and Sustainable Development, Barreiras, Bahia 47805-100, Brazil
[d] Florida Department of Transportation, Structures Design Office MS 33, Tallahassee, FL 32399, USA

ARTICLE INFO

Article history:
Received 1 June 2010
Accepted 27 September 2011
Available online 1 November 2011

Keywords:
Finite element analysis
Centrifuge testing
Spatial variability
Bearing stiffness
Soil–structure interaction

ABSTRACT

The objective of this study is to evaluate the effect of spatial variability of rock elasticity on the tip resistance of drilled shafts using experimental tests, finite element analysis (FEA) and geostatistical principles. A mathematical and computational model for simulating the multi-dimensional soil–structure interaction is developed using the ADINA FEA program and validated using data obtained from laboratory and centrifuge tests. Subsequently, the FEA model is used to quantify the spatial variability effect on the bearing stiffness of the deep foundation. Using geostatistical principles, a relationship is derived between deterministic and probabilistic end bearing stiffnesses of the rock conditions.

Published by Elsevier Ltd.

1. Introduction

Drilled shafts have been generally used as a deep foundation to carry applied axial loads by side frictional resistance on the circumference surface along its length, whereas the contribution of end bearing resistance to the load-carrying capacity of the foundation is considered to be minimal and thus neglected. However, utilizing an underlain rock layer, short but large-diameter drilled shafts are increasingly being used in practice where a substantial part of the design axial load is carried by the end bearing of the shaft [1–3]. In such a short-embedment application of drilled shafts, the bearing stiffness of the supporting rock controls foundation settlement and thus, the design of serviceability.

One method of computing the elastic settlement of a deep foundation is to use a formulation of the elastic spring equation with an influence factor to account for the stratum depth of the rock layer, which is typically assumed to be an elastic homogeneous continuum. In this deterministic approach, the elastic modulus of the rock is estimated from arithmetic averaging of mass moduli of the rock samples measured in laboratory tests. As a result, confidence in the value of an averaged elastic modulus is severely affected for design purposes by a series of uncertainties such as inherent heterogeneity of the rock [4] (i.e., random spatial variation of the elasticity) and statistical error due to small sample sizes.

Pioneering research was initiated by Fenton and Griffiths [5,6] who first adopted a geostatistical characterization of soil conditions into the finite element analysis (FEA) of the load–displacement behavior of a shallow foundation. Taking into account for the spatial variability of elastic moduli, they estimated a representative elastic modulus of the bearing soil deposits as a geometric average of random field variables of spatial correlations and, subsequently, used it in the settlement analysis of the shallow foundation. However, little work has been done on improving the deterministic approach to settlement analysis of a deep foundation. Although the design and construction of a deep foundation has introduced multi-dimensional finite element analysis to the bridge engineering industry, the increased attention to design practice such as Load and Resistance Factor Design (LRFD) has coincided with a more rigorous design criterion for the heterogeneous condition of the rock. In addition to the limited boring data available for modeling purposes, the parameter uncertainty associated with the degree of spatial variability remains unresolved within a deterministic representation of the heterogeneous nature of the rock.

This paper presents a more objective method using experimental testing and finite element analysis (FEA) to determine the bearing stiffness (i.e., the slope of the load–displacement curve at the tip) of rock-socketed drilled-shaft foundation subjected to axial loads in response to the challenge of evaluating heterogeneous rock conditions in the field. For the development of FEA models of the deep foundation, centrifuge testing is carried out using scale models to simulate load-deformation behaviors of prototypes. In addition, laboratory testing of synthetic rock specimens is

* Corresponding author. Tel.: +1 352 392 9537x1512; fax: +1 352 392 3394.
E-mail address: jchun@ce.ufl.edu (J.H. Chung).

0045-7949/$ - see front matter Published by Elsevier Ltd.
doi:10.1016/j.compstruc.2011.09.004

conducted in order to determine key material properties associated with rock constitutive models for use in FEA. Subsequently, two-dimensional axisymmetric FEA models of the prototypes are developed and calibrated against the centrifuge test results. Capable of analyzing a three-dimensional load transfer mechanism in the rock–structure interaction, calibrated FEA models are used to simulate the spatial heterogeneity of rock and its effects on bearing stiffness. As a result of a geostatistical representation of the effects, a simplified, one-dimensional bearing stiffness model of heterogeneous rock is developed using a correlation of the degree of spatial variability and a deterministic stiffness of homogeneous rock.

2. Centrifuge tests

The load-deformation behavior of the prototype rock-socketed drilled-shaft system is reproduced in a small-scale model testing where centrifugal forces would induce a similar gravitational field to which the prototype system is subjected. Two scale models of a 1.6-in. (0.04 m) diameter with lengths of 1.6 in. (0.04 m) and 4.8 in. (0.12 m) are constructed in a synthetic homogenous rock material [7], which will be referred to as Model A and Model B, respectively, throughout the remainder of the paper. Per an angular velocity of 22.5 rad/s of the centrifuge with a centrifuge arm of 4.25 ft (1.3 m), a centrifugal acceleration is approximately 67 times greater than the normal 1*g* (Fig. 1). Thus, the length and force scale factors are equal to 67 and 67^2, respectively [8,9]. In the following, test results are presented with the centrifuge model measurements multiplied by the scale relation to represent the load–displacement curves of the prototypes.

Illustrated in Fig. 2a, the load–displacement behaviors of both the models exhibit a linear trend at the tip up to a maximum displacement of 1 in. (0.0254 m), i.e., a service limit condition defined in Commentary C10.6.2.6.1 of Section 10 of Foundations of AASHTO Bridge Design Specifications [10]. Indicating material yielding

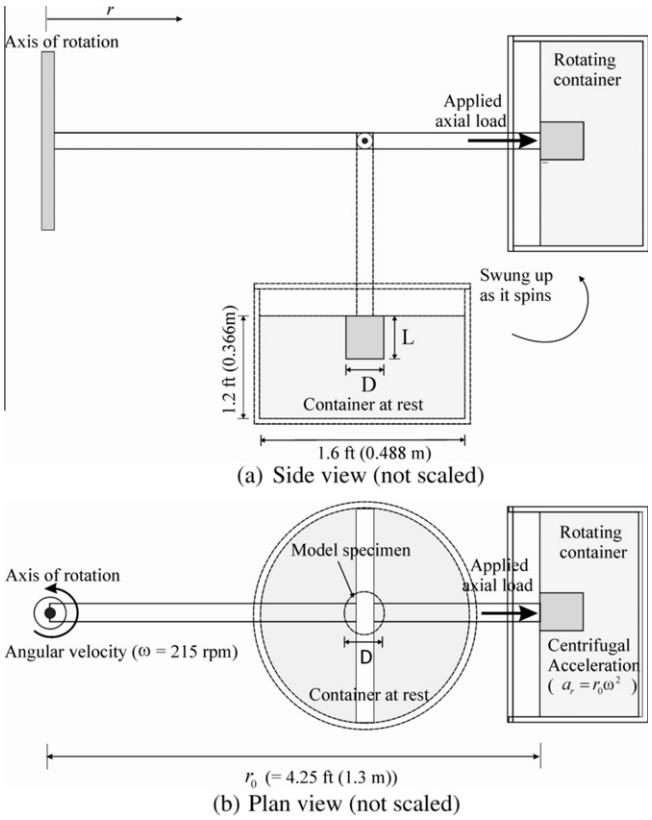

Fig. 1. Schematic sketch of the centrifuge testing.

along the side interface shown in Fig. 2b, the extrapolated side resistance of Model A appears to reach a total capacity of side resistance at the applied load of 2644 kips. In contrast, a total side resistance along a longer length of Model B has not been fully mobilized since the applied load of 4937 kips is carried by both the tip resistance of 1025 kips and the side resistance of 3912 kips. The extrapolation of the test results using the scaling relation satisfies the force equilibrium in both the models.

3. Laboratory tests

The stress–strain and strength characteristics of the synthetic rock are investigated separately in laboratory material strength tests according to the American Society for Testing and Materials (ASTM) Standards [11–13]. The purpose of the laboratory tests is to evaluate the key material parameters such as cohesion and elastic modulus of the synthetic rock for use in FEA of the prototypes. Based on the results obtained from a total of five unconfined compression tests on the synthetic rock samples, the secant elastic modulus and compressive strength of the synthetic rock are averaged to 1728 ksf (82.74 MPa) and 20 ksf (0.96 MPa), respectively. In addition, three triaxial compression and one direct shear tests are conducted to construct a Mohr's failure stress envelope (Fig. 3) where cohesion of 6 ksf (0.29 MPa) is graphically estimated using a curve fitting by a fourth-order polynominal function.

4. Finite element analysis

Numerical study described herein deals with the development of a finite element soil–structure interaction analysis model and subsequent calibration and validation of the FEA model in comparison to the centrifuge test results. For modeling nonlinear soil response and soil–structure interaction, the nonlinear implicit/explicit finite element simulation code ADINA (version 8.5) [14] is employed.

4.1. Dimensions and boundary conditions

With the scaling relation validated against the centrifuge test results, two various length-to-diameter ratios (L/D) of $L/D = 1$ and $L/D = 3$ are considered for the dimensions of the FEA models of a 9-ft (2.74 m) diameter prototype. Using symmetry for the geometry and loading conditions, two-dimensional axisymmetric FEA models are constructed. Shown in Fig. 4a is a FEA model of $L/D = 1$ where the dimensions of the FEA model are scaled by the length scale factor of 67 from those of Model A. The boundaries of the prototype FEA models are meshed by the dimensions of 3 times the shaft diameter (3D) wide and of shaft length (L) plus 3D below the shaft tip. An element size of 0.5 ft by 0.5 ft (0.1524 m by 0.1524 m) on the axisymmetry plane is used in the discretization of a synthetic homogenous limestone rock. The degree of constraint provided by the boundaries of the system is modeled such that translational motion is allowed to expand along the boundaries of the system but transversely constrained (Fig. 4a). Incremental loads up to 2726 kips (12,125 KN) for $L/D = 1$ and 4900 kips (21,794 KN) for $L/D = 3$ are applied as distributed loads to the top of the shaft. The system is assumed to be in static equilibrium prior to any applied external loads. Steel reinforcement is not considered in the FEA model development.

4.2. Constitutive models for materials

4.2.1. Concrete

In terms of determining a corresponding constitutive model for concrete, previous studies focusing on field and centrifuge tests of

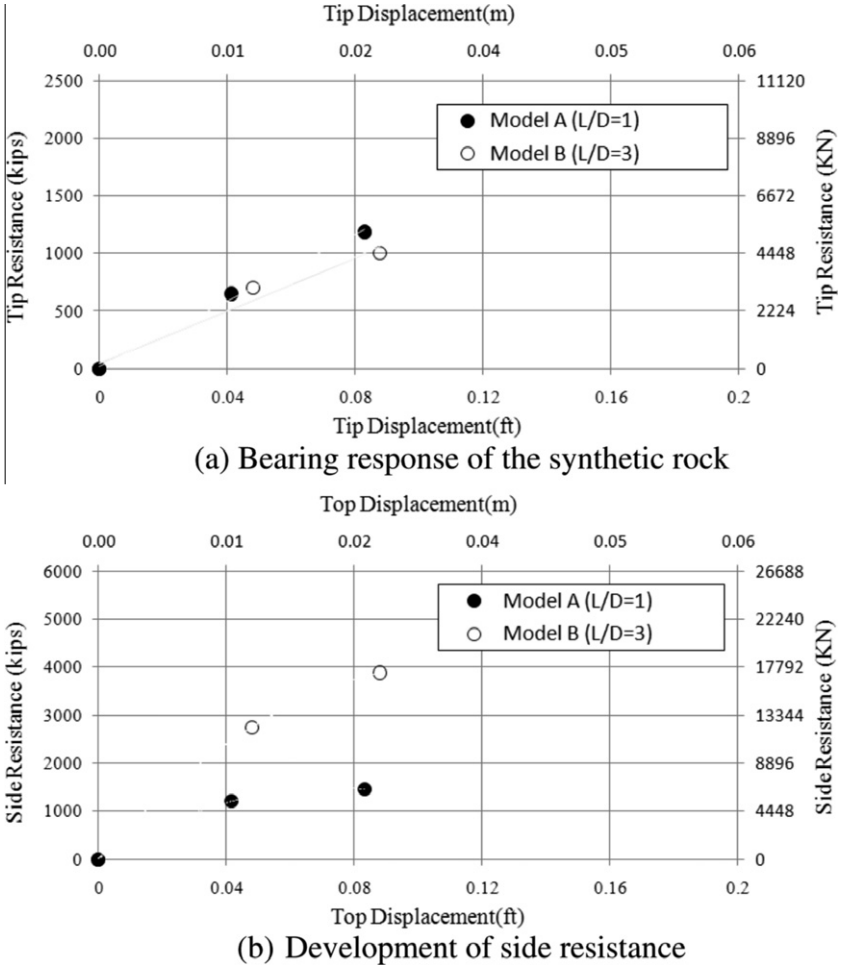

Fig. 2. Centrifuge test results.

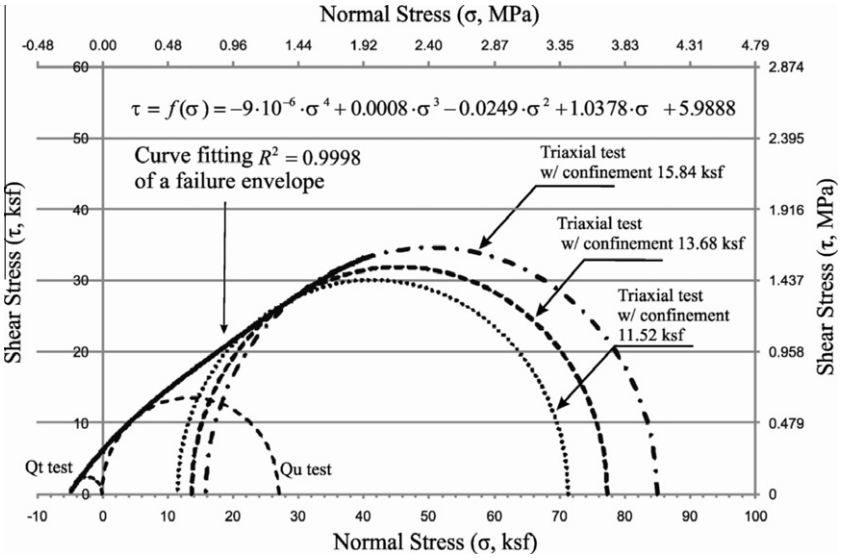

Fig. 3. Mohr's stress circles and a failure envelope.

the deep foundation subject to axial loads were reviewed [15,16]. In the range of applied axial forces to the serviceability limit, the material behavior of the concrete shaft is assumed to remain elastic. The maximum uniaxial compressive stress of the centrifuge tests is estimated to be 18 ksf (0.86 MPa), which is much lower than a 14-day compressive strength of the mortar that was used to build the scale models. Based on the review and observation, it is determined that the modified Hognestad's stress–strain relationship [17] would provide a rudimentary approximation of the elastic material behavior of the normal strength concrete.

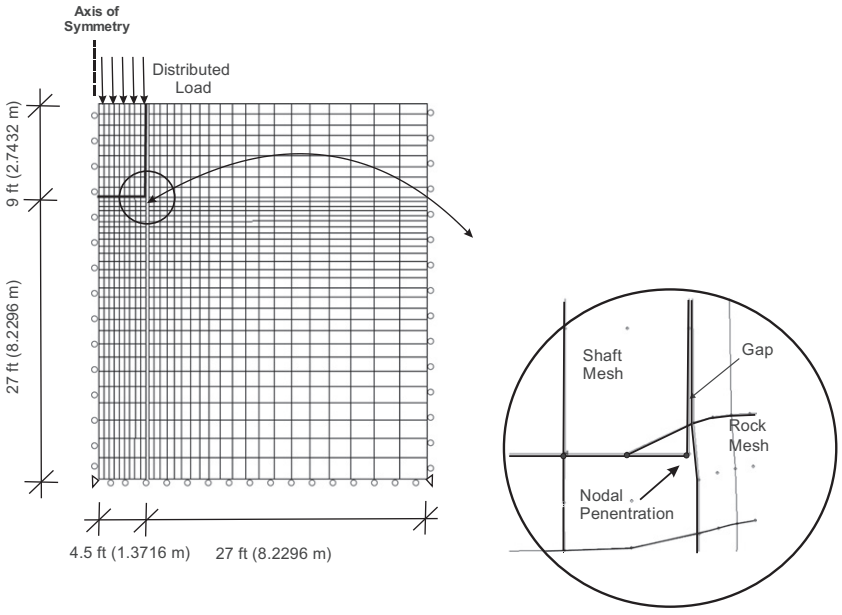

(a) Dimensions and boundary conditions of FEA model

(b) Nodal penetration

Fig. 4. Finite element analysis model and numerical instability in the contact modeling.

Significant refinement in the accuracy of the proposed concrete material model is not warranted in the current context because load-deformation of the rock-socketed drilled shafts primarily involves rock–shaft interaction where material failure of relatively weaker limestone rock more predominantly occurs along the side interface. Thus, the modeling of the interface is far more influential and important.

The key material parameters of the concrete shaft are approximated using the following assumptions [17]:

- The compressive strength of plain concrete (f_c') is approximately 5000 psi (34.5 MPa).
- The elastic modulus (E_c) is considered for static loading rather than dynamic rates of loading.
- For normal-weight concrete with a weight density of 145 lb/ft^3(2323 kgf/m^3), the elastic modulus of the concrete (E_c) can be evaluated as $E_c = 57{,}000\sqrt{f_c'}$ (psi) $\approx 4730\sqrt{f_c'}$ (MPa).

4.2.2. Synthetic rock

The ADINA soil model used in the simulation is a Mohr–Coulomb model that can predict pressure dependent failure for the rock. With the assumption of normality of a constant plastic flow to the failure surface, the plastic strain rate vector has a component in the volumetric (hydrostatic) direction that results in an increase of mean normal stresses. However, this linear postulate of the failure envelope can produce much greater shear failure stress (as minor normal stress (σ_3) increases) than what was observed in the laboratory tests. Thus, the effect that increasing normal stress has on the shear strength of the rock material is to be properly accounted for over a realistic range of maximum normal stresses that would be developed under the service loading conditions. A *tangent* slope of the failure envelope (Fig. 3) is estimated at 28° at a maximum normal stress of 18 ksf (0.86 MPa) that has been estimated at an equivalent tip displacement of 1 in. (0.0254 m) in the centrifuge tests. This tangential slope is used as the angle of friction (Φ) of the homogeneous rock. It must be noted that any prediction of nonlinear failure envelope at higher normal stresses than identified in Fig. 3 is conjecture due to the confinement restrictions of the laboratory tests. Pressure dependent failure mechanisms associated with the nonlinear failure envelope [18] should be considered to quantitatively determine accurate stress fields. Nonetheless, the material modeling approach presented here offers a practical tool calibrated with experimental data for studying a three-dimensional stress state development within the influence depth of the rock that undergoes a maximum vertical displacement of 1 in. (0.0254 m) of the service limit condition. A summary of the parameters of the rock material model is given in Table 1.

4.3. Modeling of rock–shaft interface

The rock-socketed drilled-shaft system consists of a shaft structure formed by excavation of a cylindrical borehole into the limestone rock where reinforcing steel and concrete is cast. When a shaft is subjected to axial loading, the shaft transfers the load by a combination of shear stresses developed along the cylindrical interface between the shaft and rock, and the normal stress developed at the tip of the shaft. This inelastic load-deformation mode is often seen as rock material failure along the interface based on the visual appearance that the shaft takes on after load transfer has occurred. When a shaft is designed to have sufficient axial capacity, the shaft remains structurally intact and the tip resistance contributes significant axial stiffness to the overall behavior of the rock–shaft system even after failure along the interface has occurred.

Considering the physical interface of the system constituents, the initial approach taken in modeling the interface involved the use of discrete contact edges of axisymmetric elements in which the interface represented the physical boundaries between the shaft and rock. An approximate means of accounting for the shear failure was attempted through the use of a contact model that

Table 1
Material parameters of the rock FE model.

Material parameter	Value
Poisson's ratio	0.3
Modulus of elasticity	1728 ksf (82.77 MPa)
Angle of friction (Φ)	28°
Cohesion	6 ksf (0.2874 MPa)

simulates frictional resistance under Coulomb's Law of Friction. During the contact simulations performed using this modeling technique, the approach was unfortunately found to be problematic. Nonphysical penetration at *the corner* node of the shaft into a rock element caused an artificial "gap", i.e., the rock mesh being detached from the side of the shaft (Fig. 4b) and producing zero contact force. This nonphysical penetration is a numerical instability that typically is associated with either the use of a coarse finite element mesh or too large incremental loading steps or a combination of both [19]. Under certain conditions, elements formulated using numeric integration can undergo deformation modes in which strains sampled at the element integration points fail to capture all of the strain energy associated with the deformation. As a consequence, energy is numerically (non-physically) dissipated, and the nonlinear solution process might become unstable [19,20] leading to unreliable analysis results or termination of the simulation, i.e., nonconvergence. Problems associated with nonphysical nodal penetration can often be remedied by using a high-resolution finite element mesh and small incremental loading steps. Reduction of numerical instabilities to an acceptable level (quantified by maintaining the pseudo-energy at less than 1% of total system energy) and prevention of nodal penetration *were* tried by significantly increasing the resolution of the finite element mesh and using a small loading step, e.g., an increment load of 1 kip (4.45 KN). Even with approximately 40,000 elements of the rock mesh, nodal penetration was not completely prevented. While stable solutions might be obtained, the very high-resolution mesh with such a small loading step was deemed to be impractical from the standpoint of conducting a parametric study involving numerous, repeated simulations required for the geostatistical realization of the random field condition. In preliminary analysis, several hundred simulations were found to be necessary for one geostatistical realization of a heterogeneous rock condition.

An alternative, more numerically efficient solution is achieved by abandoning the approach of modeling the contact. In the physical rock–shaft system, the circumference of the shaft is bonded to the surrounding rock. Approximate numerical modeling of this bond is accomplished using interface boundary elements (Fig. 5a). This numerical approach simulates a mathematical link between two edges together at a common interface. Parts linked together in this manner may still deform and respond to load, as may the interface between them, but the edges of the two parts remain linked to each other on a point-by-point (or node-by-node) basis (Fig. 5b). That is, at no point on the interface boundary may the two tied parts separate from each other, even though the interface boundary element itself may deform.

In contrast to the contact approach of the previous modeling technique, this approach leads to a more controlled stress redistribution of internal stresses as the rock–shaft interface yields, thus permitting stable solutions to be obtained at coarser levels of mesh resolution. Determination of the yielding, i.e., shear failure at the interface, is carried out using a Mohr–Coulomb model with the elastic–perfectly plastic yield condition such that the angle of friction (Φ) is very small, e.g., $\Phi \simeq 0$. Thus, exceedance of the failure shear stress that occurs at an integration point in an interface element was prevented by limiting a maximum shear stress to the cohesion value. This yielding mechanism permits experimentally observed amounts of deformation to be modeled and thus can produce a better representation of both the shear failure along the interface and the load transfer to the tip of the shaft.

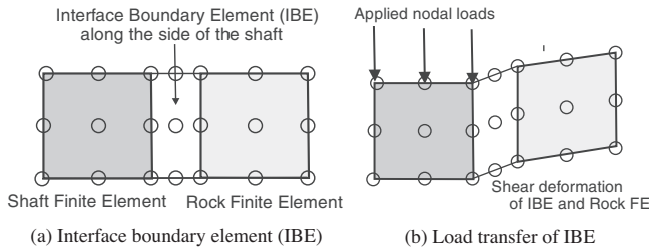

(a) Interface boundary element (IBE) (b) Load transfer of IBE

Fig. 5. Modeling of the rock–shaft side interface boundary.

4.4. Comparison between centrifuge test results and FEA predictions

The tip and side resistances for shafts of $L/D = 1$ and $L/D = 3$ predicted by finite element simulations are presented in comparison to the centrifuge test results (Fig. 6). Fig. 6a is plotted in which the summation of vertical nodal forces of the finite elements of the rock at the tip interface is compared to the tip force calculated using strain data measured at the sampling location immediately adjacent to the bottom of the centrifuge specimen.

The numerical prediction of the resultant forces at the tip (tip resistance) is shown in good agreement with the experimental measurement (Fig. 6a). In contrast, the side resistance exhibits a yield plateau where *friction resistance* reaches the limiting strength (cohesion) of the homogeneous rock (Fig. 6b). This nonlinear *trend* is evident in which the centrifuge test data fit within an acceptable margin of error. Thus, robustness (with increased numerical efficiency) of the present modeling technique, i.e., modeling of the rock–shaft interface along the embedment lengths, is validated. Also, since the rock material model has been developed using laboratory test data separate from the centrifuge tests, the agreement shown in Fig. 6 suggests a degree of validity in the load transfer mechanism both predicted by finite element simulation and measured in the centrifuge tests.

4.5. Simulations of heterogeneity

Having developed a bench-mark FEA model of the homogeneous rock condition, focus is shifted to the task of determining whether the presence of the heterogeneity is shown to affect (based on simulation results) the axial bearing resistance of the deep foundation and, if so, the extent to which point bearing response is altered by the spatial variation of the elastic modulus. Heterogeneous rock conditions are simulated in a manner to which the elastic modulus values (E_i) randomly vary per each discretized layer (i) of unit thickness (1 ft) throughout the rock mesh, while other material properties remain constant. The generation of each random distribution of the elastic modulus values is performed using the LU-decomposition method with a spherical covariance model for the Gaussian field reported in a previous study by the coauthors [21]. This skewed distribution of the spatial variability closely fits the lognormal distribution with statistics such as mean (μ_E), coefficient of variation (CV_E) and vertical correlation length (a_v) [7]. Physical meanings of these descriptive statistics are the location of the center of the distribution of the elastic modulus data, the degree of spread of the data set, and a vertical distance between two sampling layers where a distinct spatial structure of clusters of similar modulus values can be found, respectively.

Since the degree of the data spread of the elastic modulus can significantly vary from one boring site to another [7,21], lower and upper bounds of CV_E ranging from 0.2 to 0.6 with a selection of three various a_v's of 5, 10, and 15 ft are used to bound a field condition. Particularly, the selected range of CV_E is evaluated using limestone rock samples collected from the load test sites of Apalachicola and Fuller Warren Bridges located in north Florida [7]. To ensure that the predicted mean of bearing stiffness (i.e., the slope of the load–displacement curve) converges to the true mean, one-thousand random distributions are simulated per each combination of CV_E and a_v. The required number of simulations is

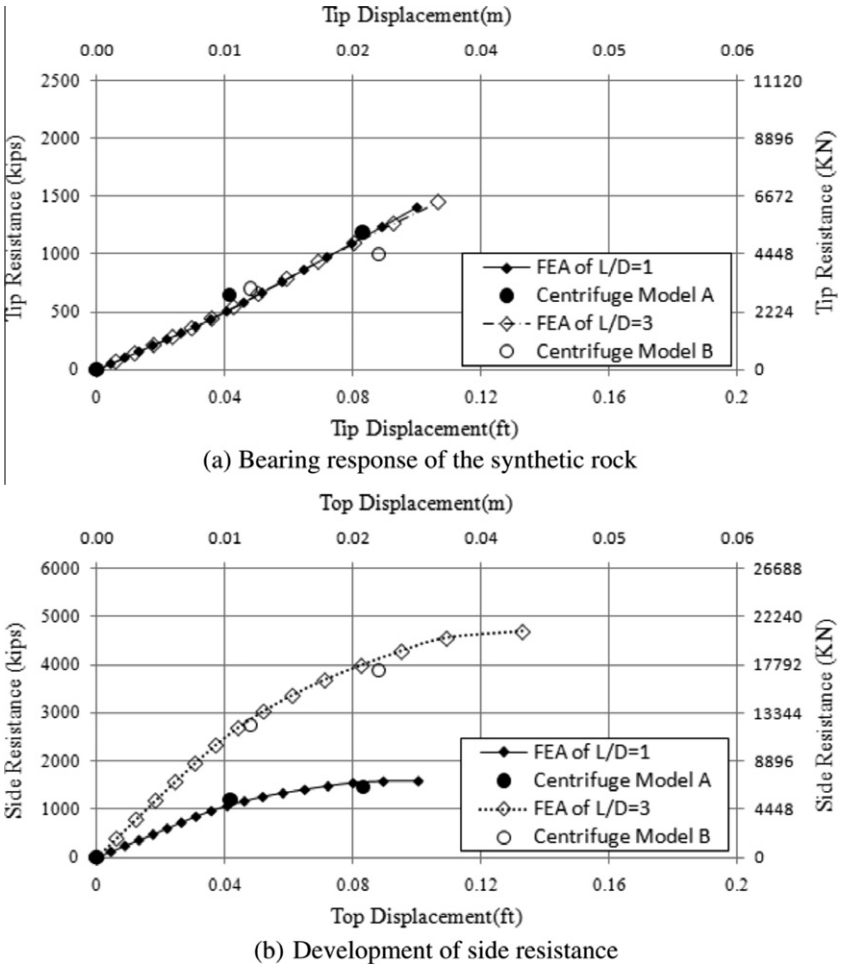

Fig. 6. Comparison of FEA with centrifuge test results.

determined to achieve a realistic representation of the field condition through geostatistical realization where the variance of the mean values collected from numerical simulations approaches zero.

Fig. 7 shows a comparison of the bearing stiffness between the homogeneous rock condition and the cases of the heterogeneous rock condition. The bearing stiffness represents the arithmetic mean of the slopes of all the load–displacement curves obtained from the 1000 simulations per each combination of various CV_E's with a constant a_v of 5 ft (1.524 m). Both the simulation results of $L/D = 1$ (left column) and $L/D = 3$ (right column) indicate that higher degrees of the variation (greater CV_E) cause a more rock "softening" effect on the tip response when compared to the homogeneous rock condition. The resultant bearing resistance decreases proportionally as CV_E increases.

In contrast, no difference in the predictions of the mean stiffness is found with respect to the variation of a_v for all the cases of CV_E ranging from 0.2 to 0.6. Basically, the load–displacement curves of the other two cases of a_v (10 ft and 15 ft) are identical to those of Fig. 7 and thus, are not repeated. This is based on no influence of these three spatial correlation lengths on the bearing stiffness being found in Fig. 8. Within the influence depth of 2D (=18 ft) [22–24], the reciprocal of the arithmetic mean of the reciprocal of a harmonic average of E_i with $CV_E = 0.2$ remains essentially constant regardless of the variation of a_v ranging from 5 ft (1.524 m) to 15 ft (4.572 m). Thus, the arithmetic mean stiffness of a heterogeneous rock is found to be insensitive to the degree of randomness but sensitive to the degree of the data spread of E_i.

5. Quantification of spatial variability effects

Based on the finding of the spatial variability, a correlation between the homogeneous and heterogeneous rock systems is derived for the prediction of the bearing stiffness. Linear regression analyses reveal that R^2 values of the bearing stiffness for both the homogeneous rock condition and each set of random distribution of E_i of the heterogeneous condition are very close to the unity. Thus, a tip displacement with respect to a random distribution of E_i is expressed proportionally to that of homogeneous rock

$$\delta_h = \frac{\delta_{\text{det}}\mu_E}{E_h} \tag{1}$$

where δ_h is a predicted tip displacement by a harmonic average of E_i, δ_{det} represents a deterministic displacement calculated using a constant elastic modulus (μ_E) of the homogeneous rock, and E_h represents a harmonic average of E_i of layer i from beneath the tip to an influence depth (H), which can be written as [25,26]

$$\frac{1}{E_h} = \frac{1}{H}\int_0^H \frac{dz}{E(z)} = \frac{1}{N}\sum_{i=1}^{N}\frac{1}{E_i} \tag{2}$$

where N represents the number of sub-layers. Recall that a single geostatistical realization in this study consists of one thousand scenarios of the random distribution of E_i. In order to numerically predict a meaningful tip displacement of the heterogeneous rock condition, the spatial variability is modeled by, not just a set of random variation, but the geostatistical realization. Thus, the *true* mean

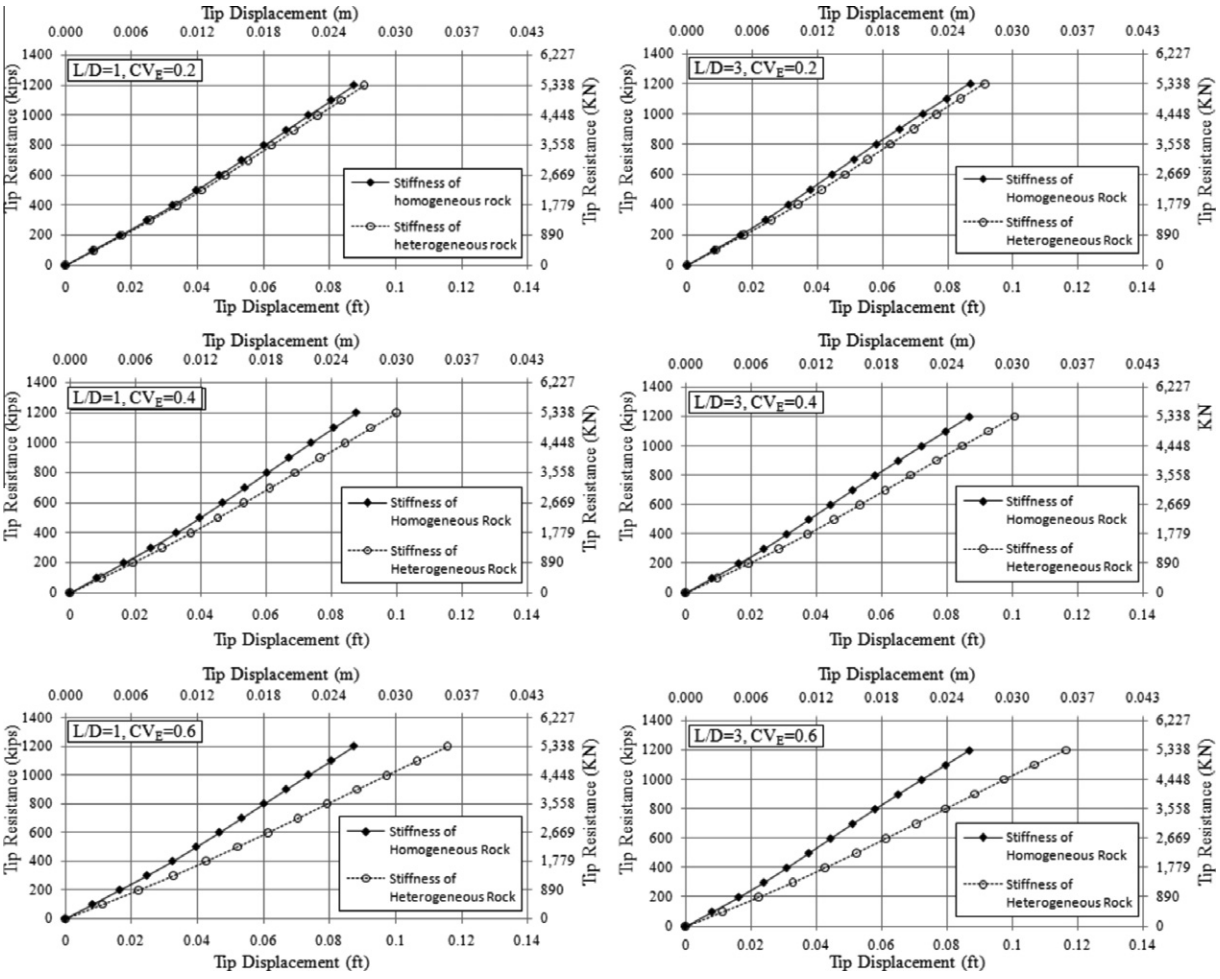

Fig. 7. Comparison of the bearing stiffness with respect to various CV_E at a_v = 5 ft.

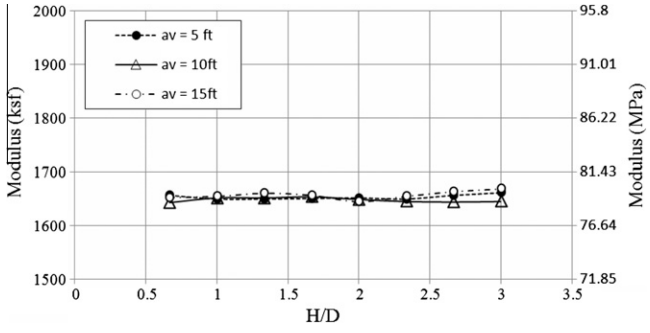

Fig. 8. Variation of the reciprocal of the arithmetic mean of $1/E_h$ with influence depths (H).

of all the harmonic means obtained from the realization should be used in Eq. (1), instead. Using a mathematical formulation given by Klammler et al. [21], the true mean of the harmonic means of the random distribution of E_i is written as

$$\mu_{Eh} = \mu_E \left(\frac{1 + \alpha \cdot CV_E^2}{1 + CV_E^2} \right) \tag{3}$$

where μ_{Eh} is the true mean of the harmonic mean moduli and α is a variance reduction factor that is applied to the harmonic averaging if μ_{Eh} fluctuates as a_v varies [26]. As noted in Fig. 8, the mean of $1/E_h$ over the influence depth of 2D remains unchanged by the variation of a_v. Thus, the variance factor drop out. As a result, Eq. (3) becomes

$$\mu_{1/E_h} = \frac{1}{\mu_E} \left(1 + CV_E^2 \right) \tag{4}$$

Where μ_{1/E_h} represents the true mean of the reciprocal of the harmonic averages (E_h). Replacing $1/E_h$ by μ_{1/E_h} in Eq. (1) and combining Eqs. (1) and (4) yields

$$\mu_{\delta h} = \delta_{\text{det}} (1 + CV_E^2) \tag{5}$$

where $\mu_{\delta h}$ is the true mean of the harmonic mean displacements. Therefore, an *effective* bearing stiffness of the heterogeneous rock (K_{eff}) can be expressed

$$K_{eff} = \frac{K_{\text{det}}}{(1 + CV_E^2)} \tag{6}$$

which quantifies the proportionality found in the finite element analysis results of Fig. 7. Considering that zero variability, i.e., $CV_E = 0$, is improbable in field conditions, the effective stiffness should always be less than the deterministic counterpart (K_{det}), depending on the degree of spatial variability.

6. Conclusion

The influence of spatial variability on rock elasticity is quantified using the probability parameter of uncertainty. A systematic approach of investigating the spatial variability using experiments

and FEA is demonstrated as a viable method for improving the design reliability of a deep foundation. Trade-off between modeling the system response at a reasonably detailed level and a desired computational efficiency as a design tool can be made in a practical application of finite element analysis in solving complex multi-dimensional soil–structure interaction problems. As a result, the present computational model—computationally efficient in its treatment of rock–shaft boundary interfaces—has been developed and validated against centrifuge test results.

The bearing stiffness of heterogeneous rock is determined by a correlation of the degree of spatial variability and a deterministic stiffness of homogeneous rock. The mean of the bearing stiffness of heterogeneous rock varies significantly with the degree of the elastic modulus data spread over the influence depth of 2D. On the other hand, whether the spatial structure of clusters of a similar value of the elastic modulus is distinct is not a contributing factor to the variation of the bearing stiffness.

Eq. (6) represents a solution for difficulties associated with the uncertainty involved in deep foundation design. With the proposed tip variance model, a side-resistance variance model could be developed by introducing another random variable of cohesion into the geostatistical realization. Although the development of bearing resistance appears to be independent of the load–displacement behavior of a rock–shaft interface subject to the service loads, variance of cohesion should be investigated to determine a total variance of the shaft resistance. If the effects of variance of cohesion are found to be independent of the variance of the elastic modulus, then the variances of the side and tip resistance can be summed to estimate a total variance of a deep foundation. Development of such models will be a major step toward reliability-based design practice of geotechnical engineering in fully utilizing the potential of Load and Resistance Factor Design (LRFD) methodology [27].

References

[1] Abu-Hejleh N, O'Neil MW, Hanneman D, Atwooll WJ. Improvement of the geotechnical axial design methodology for Colorado's drilled shafts socketed in weak rocks. Colorado Department of Transportation, Research Final Report CDOT-DTD-R-2003-6; 2003.

[2] Nusairat J, Liang RY, Engel RL. Design of rock socketed drilled shafts. Ohio Department of Transportation Research Final Report FHWA/OH-2006/21; 2006.

[3] Kansas Department of Transportation. Bridge construction manual; 2011.

[4] Goovaerts P. Geostatistics for natural resources evaluation. Oxford University Press; 1997.

[5] Fenton GA, Griffiths DV. Probabilistic foundation settlement on spatially random soil. J Geotech Geoenviron, ASCE 2002;128(5):381–90.

[6] Fenton GA, Griffiths DV. Three-dimensional probabilistic foundation settlement. J Geotech Geoenviron, ASCE 2005;131(2):232–9.

[7] McVay M, Bloomqueist D, Ko JS, Klammler H, Otero J. Distribution of end bearing and tip shear on drilled shafts founded in Florida limestone. Florida Department of Transportation, Research Final Report BD-545-59/UF 57247; 2008.

[8] Christensen SN, Bagge G. Centrifugal testing on the bearing capacity of circular footings on the surface of sand. 20th Anniversary of the Danish Engineering Academy, Danish Engineering Academy, Copenhagen, Denmark; 1977.

[9] Plizzari G, Waggoner F, Saouma VE. Centrifuge modeling and analysis of concrete gravity dams. J Struct Eng – ASCE 1995;121(10):1471–9.

[10] AASHTO LRFD bridge design specifications, 4th ed. (2009 Interim Revisions). American Association of State Highway and Transportation Officials; 2009.

[11] American Society for Testing and Materials, D2938-95. Standard test method for unconfined compressive strength of intact rock core specimens, Philadelphia, PA; 2002.

[12] American Society for Testing and Materials, D2850-03a. Standard test method for unconsolidated-undrained triaxial compression test on cohesive soils, Philadelphia, PA; 2007.

[13] American Society for Testing and Materials, D3967-95a. Standard test method for splitting tensile strength of intact rock core specimens, Philadelphia, PA; 2004.

[14] ADINA user manual, 8.5. Watertown, MA: ADINA R&D, Inc.

[15] Hsueh C, Lin S, Chen S. Lateral performance of drilled shaft considering nonlinear soil and structural material behavior. J Mar Sci Technol 2004;12(1):62–70.

[16] Ooi PSK, Lin X, Hamada HS. Numerical study of an integral abutment bridge supported on drilled shafts. J Bridge Eng 2010;15(1):19–31.

[17] MacGregor JG. Reinforced concrete. 2nd ed. Englewood cliffs, NJ: Prentice Hall; 1992.

[18] Hoek E, Brown ET. Practical estimates or rock mass strength. Int J Rock Mech Mining Sci Geomech 1997;34(8):1165–86.

[19] Bathe KJ. Finite element procedures. Upper Saddle River, NJ: Prentice Hall, Inc.; 1996.

[20] Consolazio GR, Chung JH, Gurley KR. Impact simulation and full scale crash testing of a low profile concrete work zone barrier. Comput Struct 2003;81(13):1359–74.

[21] Klammler H, McVay M, Horhota D, Lai P. Influence of spatially variable side friction on single drilled shaft resistance and LRFD resistance factors. J Geotech Eng – ASCE 2010;136(8):1114–23.

[22] Eggestad A. Deformation measurements below a model footing on the surface of dry sand. In: European conference on soil mechanics and foundation engineering, Wiesbaden, Germany; 1963. p. 233–9.

[23] Schmertmann JH, Hartman JP, Brown PR. Improved strain influence factor diagrams. J Geotech Eng – ASCE 1978;104(GT8):1131–5.

[24] Briaud J, Gibbens R. Behavior of five large spread footings in sand. J Geotech Eng – ASCE 1999;125(9):787–96.

[25] Hirai H. Settlements and stresses of multi-layered grounds and improved grounds by equivalent elastic method. Int J Numer Anal Methods Geomech 2008;32:523–57.

[26] Jensen JL, Thomas SD, Corbett PWM. On the bias and sampling variation of the harmonic average. Math Geology 1997;29(2):267–76.

[27] Paikowsky SG, Baecher GB, Ayyub B, McVay MC, Birgisson B, Kuo C. NCHRP 24-17 Load and Resistance Factor Design (LRFD) for deep foundations. Final Research Report, University of Massachusetts, Lowell, MA; 2002.